CD-MPM: Continuum Damage Material Point Methods for Dynamic Fracture Animation: Supplemental Document

Joshuah Wolper, Yu Fang, Minchen Li, Jiecong Lu, Ming Gao, Chenfanfu Jiang

Contents

1 Pseudocode

Here we present algorithms for our two approaches to dynamic fracture animation. Note that we highlight only the key differences between our routines and traditional MPM to better illustrate these contributions as MPM augmentations.

1.1 PFF-MPM Step

Algorithm 1 PFF-MPM Step

```
procedure PhaseP2G
    Compute interpolation weights, $w_{ip}^n$ //We use quadratic B-spline
    for each grid node, $i$ do
        $c_i^n = \frac{\sum_p w_{ip}^n c_p^n}{\sum_p w_{ip}^n}$
procedure PhaseSolve
    //Goal is to contruct and solve this system for $\mathbf{c}$: $(\mathcal{M} + \boldsymbol{H})\mathbf{c} = \boldsymbol{r}$
    $\boldsymbol{r} = [r_i] = \sum_p V_p^n (M_c + \frac{c_p^n}{\Delta t}) w_{ip}^n$ //Build rhs
    $\boldsymbol{H} = [\boldsymbol{H}_{ij}] = \sum_p V_p^n (4 l_0^2 M_c)(\nabla \Theta_i(\boldsymbol{x}_p^n))^T (\nabla \Theta_j(\boldsymbol{x}_p^n))$ //Build MPM discrete Laplace operator
    $\mathcal{M} = [\mathcal{M}_{ii}] = \sum_p V_p^n \left( \frac{4 l_0 M_c (1-r) \Psi_p^{\mathcal{H}}}{\mathcal{G}} + M_c + \frac{1}{\Delta t} \right) w_{ip}^n$ //Build diagonal lumped mass matrix
    Solve the system with PCG (Jacobi preconditioner takes around 4 iters)
procedure PhaseG2P
    for each particle, $p$ do
        $c_p^{n+1} = \max(0, \min(c_p^n, c_p^n + \sum_i (c_i^{n+1} - c_i^n) w_{ip}^n))$ //Prevent material healing and keep $c \in [0, 1]$
Run traditional MPM step as usual until computeForce
procedure computeForce //Key difference is this incorporates $c_p^{n+1}$
    if symplectic then
        $\boldsymbol{f}_i^n = -\sum_p V_p^0 w_{ip}^n M_p^{-1} \frac{\partial \Psi}{\partial \boldsymbol{F}} (\boldsymbol{F}_p^n, c_p^{n+1}) {\boldsymbol{F}_p^n}^T (\boldsymbol{x}_i^n - \boldsymbol{x}_p^n)$
    else if implicit then
        $\boldsymbol{f}_i^{n+1} = -\sum_p V_p^0 w_{ip}^n M_p^{-1} \frac{\partial \Psi}{\partial \boldsymbol{F}} (\boldsymbol{F}_p^{n+1}, c_p^{n+1}) {\boldsymbol{F}_p^n}^T (\boldsymbol{x}_i^n - \boldsymbol{x}_p^n)$
Finish MPM step like usual (with or without plasticity return mapping)
```

1.2 NACC Plasticity

Algorithm 2 NACC Plasticity

```
Run MPM step until we have updated elastic deformation gradients, ${F_p}^{E,n+1}$
procedure projectStrainNACC
    $U$, $\Sigma$, $V^T$ = SVD(${F_p}^{E,n+1}$)
    $p_0 = \kappa$ (0.00001 + $\xi$ sinh(max(-$\alpha$,0))) //buffer prevents YS from collapsing to a single point at 0
    $J^{E,tr} = \Sigma_{0,0} * \Sigma_{1,1} * \Sigma_{2,2}$
    $\hat{\boldsymbol{s}}^{tr} = \mu {J^{E,tr}}^{\frac{-2}{d}}$ dev($\Sigma^2$)
    $\Psi^{\kappa\prime} = \frac{\kappa}{2}(J^{E,tr} - \frac{1}{J^{E,tr}})$
    $p^{tr} = -\Psi^{\kappa\prime} J^{E,tr}$
    if $p^{tr} > p_0$ then //Case 1: Project to max tip of YS
        $J^{E,n+1} = \sqrt{\frac{-2p_0}{\kappa} + 1}$
        ${\Sigma^{n+1}}_{i,i} = {J^{E,n+1}}^{\frac{1}{d}}$ for $i$ = 0, 1, 2
        $\alpha$ += log($\frac{J^{E,tr}}{J^{E,n+1}}$)
        return $U * \Sigma^{n+1} * V^T$
    if $p^{tr} < -\beta p_0$ then //Case 2: Project to min tip of YS
        $J^{E,n+1} = \sqrt{\frac{2\beta p_0}{\kappa} + 1}$
        ${\Sigma^{n+1}}_{i,i} = {J^{E,n+1}}^{\frac{1}{d}}$ for $i$ = 0, 1, 2
        $\alpha$ += log($\frac{J^{E,tr}}{J^{E,n+1}}$)
        return $U * \Sigma^{n+1} * V^T$
    $y = (1+2\beta)(\frac{6-d}{2})||\hat{\boldsymbol{s}}^{tr}|| + M^2(p^{tr} + \beta p_0)(p^{tr} - p_0)$
    if $y < 0.0001$ then //Inside YS
        return $U * \Sigma * V^T$
    if $p_0 > 0.0001$ and $p^{tr} < p_0 - 0.0001$ and $p^{tr} > -\beta p_0 + 0.0001$ then //Case 3: Hardening Routine
        $p^c = (1-\beta)\frac{p_0}{2}$
        $q^{tr} = \sqrt{\frac{6-d}{2}}||\hat{\boldsymbol{s}}^{tr}||$
        $direction[0] = p^c - p^{tr}$
        $direction[1] = 0 - q^{tr}$
        $direction = \frac{direction}{||direction||}$
        $C = M^2(p^c + \beta p_0)(p^c - p_0)$
        $B = M^2 direction[0](2p^c - p_0 + \beta p_0)$
        $A = M^2 direction[0]^2 + (1+2\beta)direction[1]^2$
        $l_1 = \frac{-B+\sqrt{B^2-4AC}}{2A}$
        $l_2 = \frac{-B-\sqrt{B^2-4AC}}{2A}$
        $p_1 = p^c + l_1 direction[0]$
        $p_2 = p^c + l_2 direction[0]$
        $p^\times = (p^{tr} - p^c)(p_1 - p^c)$ ? $p_1$ : $p_2$
        $J^{E,\times} = \sqrt{\frac{-2p^\times}{\kappa} + 1}$
        if $J^{E,\times} > 0.0001$ then
            $\alpha$ += log($\frac{J^{E,tr}}{J^{E,\times}}$)
    //Case 3: Yield Surface Projection
    $\hat{\boldsymbol{b}}^{E,n+1} = \sqrt{\frac{-M^2(p^{tr}+\beta p_0)(p^{tr}-p_0)}{(1+2\beta)(\frac{6-d}{2})}}(\frac{{J^{E,tr}}^{\frac{2}{d}}}{\mu})\frac{\hat{\boldsymbol{s}}^{tr}}{||\hat{\boldsymbol{s}}^{tr}||} + \frac{1}{d}$trace($\Sigma^2$)
    ${\Sigma^{n+1}}_{i,i} = \sqrt{\hat{\boldsymbol{b}}_i^{E,n+1}}$ for $i$ = 0, 1, 2
    return $U * \Sigma^{n+1} * V^T$
```

2 Incremental Potential and Euler-Lagrangian Equations

2.1 Momentum Conservation

We focus on the response of hyper-elastoplastic solids, where the backward Euler time integration from t^n to t^{n+1} can be recast into a variational problem [14] minimizing an incremental energy in the material space Ω^0. For our degraded hyperelastic object, the *incremental* elastic energy density in terms of the unknown t^{n+1} deformation map is defined as

$$W(\boldsymbol{F}^{n+1}, c^{n+1}) = \Psi(\boldsymbol{F}^{n+1}, c^{n+1}) - \Psi(\boldsymbol{F}^n, c^n). \tag{1}$$

Let's lag the effect of the phase-field and assume $c^{n+1} = c^n$ and $W = W(\boldsymbol{F}^{n+1})$ (pure hyperelasticity). In this case, Radovitzky and Ortiz [14] proposed the following incremental potential energy for backward Euler:

$$\begin{aligned}\mathcal{I}(\phi^{n+1}) = &\int_{\Omega^0} \left(\frac{1}{2} \frac{R}{\Delta t^2} |\phi^{n+1}|^2 + W(\boldsymbol{F}^{n+1}) \right) d\boldsymbol{X} \\ &- \int_{\Omega^0} \left(\boldsymbol{f}^{ext} + R \frac{\hat{\phi}}{\Delta t^2} \right) \cdot \phi^{n+1} d\boldsymbol{X} - \int_{\partial\Omega^0} \boldsymbol{T}^{n+1} \cdot \phi^{n+1} dS,\end{aligned} \tag{2}$$

where $\hat{\phi} = \phi^n + \Delta t \frac{\partial \phi}{\partial t}^n$ with $\boldsymbol{V} = \frac{\partial \phi}{\partial t}$ being the Lagrangian velocity, $R(\boldsymbol{X}, t)$ being the Lagrangian density, $\boldsymbol{f}^{\text{ext}}$ being the external force per unit volume (such as gravity $R\boldsymbol{g}$), and $\boldsymbol{T}^{n+1}$ being the prescribed traction boundary condition at t^{n+1} (which we assume is zero for the following derivation). The optimal ϕ^{n+1} can be found by solving the variational problem [14]

$$\mathcal{I}(\phi^{n+1}) = \inf_{\tilde{\phi}} \mathcal{I}(\tilde{\phi}), \tag{3}$$

which requires computing the variational derivative of the functional $\mathcal{I}(\phi)$. Denoting the integrand in $\mathcal{I}(\phi^{n+1})$ with $\mathcal{L}(\phi, \nabla^{\boldsymbol{X}} \phi)$ where $\nabla^{\boldsymbol{X}} \phi = \boldsymbol{F}$, we can easily write the Euler-Lagrangian form of Eqn. (2)

$$\frac{\partial \mathcal{L}}{\partial \phi} - \frac{d}{d\boldsymbol{X}} \frac{\partial \mathcal{L}}{\partial \nabla^{\boldsymbol{X}} \phi} = 0,$$

which reveals the Lagrangian momentum conservation

$$\frac{R}{\Delta t^2} \phi^{n+1} - \nabla^{\boldsymbol{X}} \cdot \boldsymbol{P}^{n+1} = \boldsymbol{f}^{\text{ext}} + \frac{R}{\Delta t^2} (\phi^n + \Delta t \boldsymbol{V}^n), \tag{4}$$

where $\boldsymbol{P}^{n+1} = \frac{\partial \Psi}{\partial \boldsymbol{F}}(\boldsymbol{F}^{n+1})$ is the first Piola-Kirchhoff stress. Note that with implicit Euler, the advection of the deformation mapping is given by $\phi^{n+1} = \phi^n + \Delta t \boldsymbol{V}^{n+1}$, which also allows us to reformulate Eqn. (4) in terms of velocities.

2.2 Phase-Field Evolution

2.2.1 Parabolic Phase-field Evolution

To avoid the problems with local damage mechanics, we target a phase-field evolution rule that is constructed using the Ginzburg-Landau theory [13] following general thermodynamics and kinetics.

Since we want to solve our phase-field governing equation with backward Euler, we propose a phase-field enhanced incremental potential by augmenting Eqn. (2) with additional inertia terms related to c (note that we have omitted the traction boundary term):

$$\begin{aligned}&\mathcal{I}(c^{n+1}, \phi^{n+1}) \\ &= \int_{\Omega^0} \left(\frac{1}{2} \frac{R_c}{\Delta t} |c^{n+1}|^2 + \frac{1}{2} \frac{R}{\Delta t^2} |\phi^{n+1}|^2 + W(\boldsymbol{F}^{n+1}, c^{n+1}) \right) d\boldsymbol{X} \\ &- \int_{\Omega^0} \left(\boldsymbol{f}^{ext} + R \frac{\hat{\phi}}{\Delta t^2} \right) \cdot \phi^{n+1} d\boldsymbol{X} - \int_{\Omega^0} \frac{R_c}{\Delta t} c^n c^{n+1} d\boldsymbol{X},\end{aligned} \tag{5}$$

where $R_c(\boldsymbol{X},t)$, similarly to mass density R, controls the balancing ratio between the phase-field inertia and the elastic energy. Similarly to before, we denote the integrand of $\mathcal{I}(c,\phi)$ with $\mathcal{L}(c,\nabla^{\boldsymbol{X}}c,\phi,\nabla^{\boldsymbol{X}}\phi)$. The Euler-Lagrangian equation for $c^{n+1}(\boldsymbol{X})$ (given by $\frac{\partial\mathcal{L}}{\partial c}-\frac{d}{d\boldsymbol{X}}\frac{\partial\mathcal{L}}{\partial\nabla^{\boldsymbol{X}}c}=0$) reveals

$$\left(\frac{4l_0M_c(1-r)\Psi^+}{\mathcal{G}}+M_c+\frac{1}{\Delta t}\right)c^{n+1}-(4l_0^2M_c)\nabla^2c^{n+1}=M_c+\frac{c^n}{\Delta t}, \tag{6}$$

where $M_c=\mathcal{G}/(2R_cl_0)$ is a material parameter, and ∇^2 is the Laplace operator with respect to $\boldsymbol{X}$.

2.2.2 Alternative derivation with functional derivatives

Note that our result is consistent with the dynamic Ginzburg-Landau type evolution equation proposed by Kuhn and Müller [12] as

$$\frac{Dc}{Dt}=-\hat{M}\frac{\delta\mathcal{E}}{\delta c}, \tag{7}$$

where $\hat{M}$ is a scaled version of our M_c that controls the viscosity of crack propagation and is usually measured empirically. $\frac{\delta\mathcal{E}}{\delta c}$ is the functional derivative of the free energy. Note that we use $c(\boldsymbol{x},t)$ and $c(\boldsymbol{X},t)$ to denote Eulerian and Lagrangian phase-field quantities respectively throughout the paper, with the understanding that all Lagrangian quantities are pushed forward into their Eulerian counterparts to enable an MPM discretization.

The Eulerian governing PDE for c thus boils down to computing the functional derivative $\frac{\delta\mathcal{E}}{\delta c}$.

$$\mathcal{E}=\int_{\Omega^t}g(c)\Psi^++\Psi^-+\left(\frac{(c-1)^2}{4l_0}+l_0|\nabla^{\boldsymbol{x}}c|^2\right)\mathcal{G}d\boldsymbol{x},$$

where $g(c)=(1-r)c^2+r$. We can compute its functional derivative [5] to get

$$\frac{\delta\mathcal{E}[c]}{\delta c(\boldsymbol{x})}=(2(1-r)c)\Psi^++\frac{c-1}{2l_0}\mathcal{G}-2l_0\mathcal{G}\nabla^2c.$$

By defining $M_c=\frac{\hat{M}}{2l_0}\mathcal{G}$, we observe the equivalence between Eq. 7 and Eq. 6.

3 MLS-MPM Implicit Phase-Field Solver

3.1 Weak Form

Our goal is to use MPM to discretize the Backward Euler form of the parabolic phase-field evolution equation. In particular, we use Moving Least Squares MPM shape functions [9] due to their superior efficiency and ease of implementation. The Lagrangian governing equation is given by:

$$\left(\frac{4l_0M_c(1-r)\psi^{\mathcal{H}}}{\mathcal{G}}+M_c+\frac{1}{\Delta t}\right)c^{n+1}-(4l_0^2M_c)\nabla^2c^{n+1}=M_c+\frac{c^n}{\Delta t}.$$

The Eulerian weak form of this PDE is

$$\int_{\Omega^t}\omega((\alpha-\beta\nabla^2)c^{n+1}-\gamma)d\boldsymbol{x}=0,$$

where $\alpha(\boldsymbol{x},t)$, $\beta(\boldsymbol{x},t)$, and $\gamma(\boldsymbol{x},t)$ are the corresponding coefficients, and $\omega(\boldsymbol{x},t)$ is an arbitrary test function.

We follow the same way of discretizing the momentum equation using a Galerkin style weak form [10] and take an updated Lagrangian view by looking at t^n.

3.2 MLS Shape Functions

For any test function $w(\boldsymbol{x}, t^n)$ in the proper function space, the time discretization reveals

$$\int_{\Omega^{t^n}} w(\boldsymbol{x}, t^n)\{(\alpha(\boldsymbol{x}, t^n) - \beta(\boldsymbol{x}, t^n)\nabla^2)c(\boldsymbol{x}, t^{n+1}) - \gamma(\boldsymbol{x}, t^n)\}d\boldsymbol{x} = 0$$

$$\int_{\Omega^{t^n}} w(\boldsymbol{x}, t^n)\{\alpha(\boldsymbol{x}, t^n)c(\boldsymbol{x}, t^{n+1}) - \gamma(\boldsymbol{x}, t^n)\}d\boldsymbol{x} - \int_{\partial\Omega^{t^n}} \beta(\boldsymbol{x}, t^n)w(\boldsymbol{x}, t^n)\nabla c(\boldsymbol{x}, t^{n+1}) \cdot \boldsymbol{n}ds$$
$$- \int_{\Omega^{t^n}} \beta(\boldsymbol{x}, t^n)(\nabla w(\boldsymbol{x}, t^n)) \cdot (\nabla c(\boldsymbol{x}, t^{n+1}))d\boldsymbol{x} = 0$$

and the second equation is achieved by applying integration by parts to the term with the Laplace operator. Additionally, the surface integral term can be set to zero by carefully choosing the test function:

$$\int_{\Omega^{t^n}} w(\boldsymbol{x}, t^n)\{\alpha(\boldsymbol{x}, t^n)c(\boldsymbol{x}, t^{n+1}) - \gamma(\boldsymbol{x}, t^n)\}d\boldsymbol{x} + \int_{\Omega^{t^n}} \beta(\boldsymbol{x}, t^n)(\nabla w(\boldsymbol{x}, t^n)) \cdot (\nabla c(\boldsymbol{x}, t^{n+1}))d\boldsymbol{x} = 0$$

The next step is MLS style spacial discretization. Following [9], we adopt the MLS shape function $\Theta_{\mathbf{i}}(\boldsymbol{x})$ at each node near a particle to discretize both the test function and the physical fields. That is, we do

$$w^n = w^n_{\mathbf{i}}\Theta_{\mathbf{i}}, \quad c^n = c^n_{\mathbf{j}}\Theta_{\mathbf{j}}, \quad c^{n+1} = c^{n+1}_{\mathbf{j}}\Theta_{\mathbf{j}}. \tag{8}$$

and notice that c^n has been embedded in γ. We refer to [9] for the construction of the MLS shape functions in a way that is consistent with Element Free Galerkin (EFG) methods.

Then,

$$\int_{\Omega^{t^n}} w^n_{\mathbf{i}}\Theta_{\mathbf{i}}\alpha(\boldsymbol{x}, t^n)c^n_{\mathbf{j}}\Theta_{\mathbf{j}}d\boldsymbol{x} + \int_{\Omega^{t^n}} \beta(\boldsymbol{x}, t^n)(w^n_{\mathbf{i}}\nabla\Theta_{\mathbf{i}}) \cdot (c^n_{\mathbf{j}}\nabla\Theta_{\mathbf{j}})d\boldsymbol{x} = \int_{\Omega^{t^n}} w^n_{\mathbf{i}}\Theta_{\mathbf{i}}\gamma(\boldsymbol{x}, t^n)d\boldsymbol{x} \tag{9}$$

Utilizing the MLS shape functions avoids differentiating B-spline kernels in high dimensions. More specifically, if a linear polynomial space with quadratic B-spline weighting is chosen for the MLS reconstruction, we have [9]

$$\nabla\Theta_{\mathbf{i}}(\boldsymbol{x}_p) = D_p^{-1}N_{\mathbf{i}}(\boldsymbol{x}^n_p)(\boldsymbol{x}_{\mathbf{i}} - \boldsymbol{x}^n_p),$$

where $D_p = \frac{1}{4}\Delta x^2$ for quadratic B-spline weighting in $N_{\mathbf{i}}(\boldsymbol{x})$.

3.3 Lumped Mass

Similarly to how the mass matrix was defined in the momentum case, we can define a "phase field mass" matrix

$$\boldsymbol{M}^n_{\mathbf{ij}} = \int_{\Omega^{t^n}} \Theta_{\mathbf{i}}(\boldsymbol{x})\alpha(\boldsymbol{x}, t^n)\Theta_{\mathbf{j}}(\boldsymbol{x})d\boldsymbol{x}$$

Adopting one point quadrature over particle domains

$$\approx \sum_p V^n_p \alpha_p \Theta_{\mathbf{i}}(\boldsymbol{x}_p)\Theta_{\mathbf{j}}(\boldsymbol{x}_p)$$

where V^n_p is the current volume for particle p.

Now we can rewrite Equation (9) as

$$\boldsymbol{M}^n_{\mathbf{ij}}w^n_{\mathbf{i}}c^n_{\mathbf{j}} + \int_{\Omega^{t^n}} \beta(w^n_{\mathbf{i}}\nabla\Theta_{\mathbf{i}}) \cdot (c^n_{\mathbf{j}}\nabla\Theta_{\mathbf{j}})d\boldsymbol{x} = \int_{\Omega^{t^n}} w^n_{\mathbf{i}}\Theta_{\mathbf{i}}\gamma(\boldsymbol{x}, t^n)d\boldsymbol{x}$$

and choose

$$w^n_{\mathbf{i}} = \begin{cases} 1, & \mathbf{i} = \hat{\mathbf{i}} \\ 0, & \text{otherwise} \end{cases}$$

then we have, for each node $\hat{\mathbf{i}}$,

$$\boldsymbol{M}^n_{\hat{\mathbf{i}}\mathbf{j}} c^n_{\mathbf{j}} + \int_{\Omega^{t^n}} \beta(\nabla\Theta_{\hat{\mathbf{i}}}) \cdot (c^n_{\mathbf{j}} \nabla\Theta_{\mathbf{j}}) d\boldsymbol{x} = \int_{\Omega^{t^n}} \Theta_{\hat{\mathbf{i}}} \gamma(\boldsymbol{x}, t^n) d\boldsymbol{x} \tag{10}$$

We can further apply the mass lumping strategy to reduce a full mass matrix into a diagonal matrix. Let's call each new entry $\hat{\boldsymbol{M}}^n_{\hat{\mathbf{i}}}$, then

$$\begin{aligned}
\hat{\boldsymbol{M}}^n_{\mathbf{i}} &= \sum_{\mathbf{j}} \boldsymbol{M}^n_{\mathbf{i}\mathbf{j}} \\
&= \sum_{\mathbf{j}} \int_{\Omega^{t^n}} \Theta_{\mathbf{i}}(\boldsymbol{x}) \alpha(\boldsymbol{x}, t^n) \Theta_{\mathbf{j}}(\boldsymbol{x}) d\boldsymbol{x} \\
&= \int_{\Omega^{t^n}} \Theta_{\mathbf{i}}(\boldsymbol{x}) \alpha(\boldsymbol{x}, t^n) d\boldsymbol{x} \\
&\approx \sum_p V_p \alpha_p \Theta_{\mathbf{i}}(\boldsymbol{x}_p).
\end{aligned}$$

We use $\boldsymbol{M}^n_{\hat{\mathbf{i}}\mathbf{j}} \approx \hat{\boldsymbol{M}}^n_{\hat{\mathbf{i}}} \delta_{\hat{\mathbf{i}}\mathbf{j}}$ to rewrite Equation 9:

$$\hat{\boldsymbol{M}}^n_{\hat{\mathbf{i}}} c^n_{\hat{\mathbf{i}}} + \int_{\Omega^{t^n}} \beta(\nabla\Theta_{\hat{\mathbf{i}}}) \cdot (c^n_{\mathbf{j}} \nabla\Theta_{\mathbf{j}}) d\boldsymbol{x} = \int_{\Omega^{t^n}} \Theta_{\hat{\mathbf{i}}} \gamma(\boldsymbol{x}, t^n) d\boldsymbol{x} \tag{11}$$

Let's replace $\hat{i}$ with i to get the final equation for the phase field on node $\mathbf{i}$:

$$\hat{\boldsymbol{M}}^n_{\mathbf{i}} c^n_{\mathbf{i}} + \int_{\Omega^{t^n}} \beta(\nabla\Theta_{\mathbf{i}}) \cdot (c^n_{\mathbf{j}} \nabla\Theta_{\mathbf{j}}) d\boldsymbol{x} = \int_{\Omega^{t^n}} \Theta_{\mathbf{i}} \gamma(\boldsymbol{x}, t^n) d\boldsymbol{x} \tag{12}$$

3.4 The force term

The right side of Eqn. (12) is:

$$\int_{\Omega^{t^n}} \Theta_{\mathbf{i}} \gamma(\boldsymbol{x}, t^n) d\boldsymbol{x} \approx \sum_p \Theta_i(\boldsymbol{x}_p) \gamma(\boldsymbol{x}_p, t^n) V^n_p. \tag{13}$$

And the only term left is the so-called 'internal force':

$$\begin{aligned}
\int_{\Omega^{t^n}} \beta(\boldsymbol{x}, t^n)(\nabla\Theta_{\mathbf{i}}(\boldsymbol{x}_p)) \cdot (c^n_{\mathbf{j}} \nabla\Theta_{\mathbf{j}}(\boldsymbol{x}_p)) d\boldsymbol{x} &\approx \sum_p \beta(\boldsymbol{x}_p, t^n)(\nabla\Theta_{\mathbf{i}}(\boldsymbol{x}_p)) \cdot (c^n_{\mathbf{j}} \nabla\Theta_{\mathbf{j}}(\boldsymbol{x}_p)) V^n_p \\
&= \sum_p \sum_{\mathbf{j}} \beta(\boldsymbol{x}_p, t^n)(\nabla\Theta_{\mathbf{i}}(\boldsymbol{x}_p)) \cdot (c^n_{\mathbf{j}} \nabla\Theta_{\mathbf{j}}(\boldsymbol{x}_p)) V^n_p \\
&= \sum_{\mathbf{j}} [\sum_p \beta(\boldsymbol{x}_p, t^n) V^n_p (\nabla\Theta_{\mathbf{i}}(\boldsymbol{x}_p)) \cdot (\nabla\Theta_{\mathbf{j}}(\boldsymbol{x}_p))] c^n_{\mathbf{j}} \\
&= \sum_{\mathbf{j}} \boldsymbol{H}_{\mathbf{i}\mathbf{j}} c^n_{\mathbf{j}}
\end{aligned}$$

where $\boldsymbol{H}_{\mathbf{i}\mathbf{j}} = \sum_p \beta(\boldsymbol{x}_p, t^n) V^n_p (\nabla\Theta_{\mathbf{i}}(\boldsymbol{x}_p)) \cdot (\nabla\Theta_{\mathbf{j}}(\boldsymbol{x}_p))$.

3.5 Summary

Finally, let's summarize the implicit formulation of the phase field assuming no boundary flux:

$$(\boldsymbol{M} + \boldsymbol{H})\mathbf{c} = \boldsymbol{r} \tag{14}$$

where $\mathbf{c}$ is the vector of all nodal unknowns of phase field, $\boldsymbol{M}$ is diagonal mass matrix, $\boldsymbol{H}$ is an MPM-based discrete Laplace operator, and $\boldsymbol{r}$ is the right hand side as in Eqn. (13). The resulting implicit system is positive semidefinite and can be efficiently solved with the standard Conjugate Gradient solver with a diagonal preconditioner.

4 Elasticity

In this section, all $\boldsymbol{F}$, J, etc. are assumed to be the elastic quantities with superscript "E" omitted.

4.1 Energy

The energy density of the Neo-Hookean model [19] is

$$\begin{aligned}
\Psi^{\mu}(\boldsymbol{F}) &= \frac{\mu}{2}(\mathrm{tr}(\boldsymbol{F}^T\boldsymbol{F}) - d) \qquad (15)\\
\Psi^{\kappa}(J) &= \frac{\kappa}{2}(\frac{J^2-1}{2} - \log(J))\\
\hat{\Psi} &= \Psi^{\mu}(\boldsymbol{F}) + \Psi^{\kappa}(J)
\end{aligned}$$

where μ and $\kappa = \frac{2}{3}\mu + \lambda$ are shearing and bulk modulus. Similar to [17], we first decompose the deformation gradient into the deviatoric and dilational/volumetric parts as:

$$\begin{aligned}
\boldsymbol{F} &= \boldsymbol{F}^{\mathrm{dev}}\boldsymbol{F}^{\mathrm{vol}}\\
\boldsymbol{F}^{\mathrm{dev}} &= (J)^{-\frac{1}{d}}\boldsymbol{F}\\
\boldsymbol{F}^{\mathrm{vol}} &= (J)^{\frac{1}{d}}\boldsymbol{I};
\end{aligned}$$

Second, we change the definition of energy density by replacing $\Psi^{\mu}(\boldsymbol{F})$ with $\Psi^{\mu}(J^a\boldsymbol{F})$ where $a = -\frac{1}{d}$; thus, the new energy is:

$$\Psi = \Psi^{\mu}(J^a\boldsymbol{F}) + \Psi^{\kappa}(J).$$

Since the first term relies only on $\boldsymbol{F}^{\mathrm{dev}}$ while the second term relies only on $\boldsymbol{F}^{\mathrm{vol}}$ (i.e. J), we can re-label them as

$$\Psi = \Psi^{\mathrm{dev}}(J^a\boldsymbol{F}) + \Psi^{\mathrm{vol}}(J).$$

Furthermore, we define

$$\Psi^{+} = \begin{cases} \Psi^{\mathrm{dev}}(J^a\boldsymbol{F}) + \Psi^{\mathrm{vol}}(\boldsymbol{F}) & J \geq 1 \\ \Psi^{\mathrm{dev}}(J^a\boldsymbol{F}) & J < 1 \end{cases}, \quad \Psi^{-} = \begin{cases} 0 & J \geq 1 \\ \Psi^{\mathrm{vol}}(\boldsymbol{F}) & J < 1 \end{cases}$$

where Ψ^{+} can be penalized by a factor of $g(c)$ while keeping the Ψ^{-} unchanged. This is visualized in Fig. 1 both through varying the phase variable, c, and through decomposing the total energy into its components for a single c value.

4.2 Stress

We compute the stress for both components separately.

4.2.1 Deviatoric stress

$$\boldsymbol{P}^{\mathrm{dev}} = \left.\frac{\partial\Psi^{\mathrm{dev}}}{\partial\boldsymbol{F}}\right|_{J^a\boldsymbol{F}} : \frac{\partial(J^a\boldsymbol{F})}{\partial\boldsymbol{F}}$$

The left part is easy to show by putting δ on Eqn. (15):

$$\begin{aligned}
\delta\Psi^{\mu} &= \frac{\mu}{2}\delta(\boldsymbol{F}:\boldsymbol{F})\\
&= \mu\boldsymbol{F}:\delta\boldsymbol{F},
\end{aligned}$$

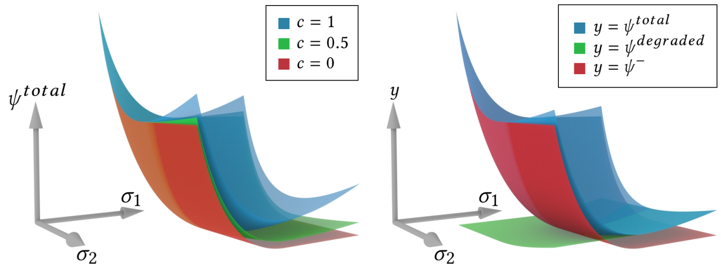

Figure 1: **Split Energy Density with Degradation.** (Left) Total energy, $\Psi^{\text{total}} = \Psi$, plotted for three damage values; note the overlapping energies when σ_1 and σ_2 are below 1. (Right) Decomposition of Ψ into its components, $\Psi^{\text{degraded}} = g(c)\Psi^{+}$ and Ψ^{-}.

thus $\frac{\partial \Psi^{\mu}}{\partial \boldsymbol{F}} = \mu \boldsymbol{F}$. The right part can be derived,

$$\begin{aligned}\frac{\partial (J^a \boldsymbol{F})}{\partial \boldsymbol{F}} &= \boldsymbol{F}\frac{\partial (J^a)}{\partial \boldsymbol{F}} + J^a \frac{\partial (\boldsymbol{F})}{\partial \boldsymbol{F}} \\ &= J^a (a\boldsymbol{F}\boldsymbol{F}^{-T} + \boldsymbol{I}^{4th})\end{aligned}$$

where $\boldsymbol{I}^{4th}$ is the fourth order identity tensor which can be defined as

$$\boldsymbol{I}^{4th} = \delta_{ik}\delta_{jl}\boldsymbol{e}_i \otimes \boldsymbol{e}_j \otimes \boldsymbol{e}_k \otimes \boldsymbol{e}_l,$$

and we used

$$\frac{\partial J}{\partial \boldsymbol{F}} = J\boldsymbol{F}^{-T}.$$

Thus we can get,

$$\begin{aligned}\boldsymbol{P}^{\text{dev}} &= \mu J^a \boldsymbol{F} : J^a (a\boldsymbol{F}\boldsymbol{F}^{-T} + \boldsymbol{I}^{4th}) \\ &= \mu J^{2a}(a\boldsymbol{F} : \boldsymbol{F}\boldsymbol{F}^{-T} + \boldsymbol{F}).\end{aligned} \tag{16}$$

Remember Kirchhoff stress is defined as $\boldsymbol{\tau}^{\text{dev}} = \boldsymbol{P}^{\text{dev}}\boldsymbol{F}^T$,

$$\begin{aligned}\boldsymbol{\tau}^{\text{dev}} &= \mu J^{2a}(a \ \text{tr}(\boldsymbol{b})\boldsymbol{I} + \boldsymbol{b}) \\ &= \mu J^{-\frac{2}{d}}(\boldsymbol{b} - \frac{1}{d}\text{tr}(\boldsymbol{b})\boldsymbol{I}) \\ &= \mu J^{-\frac{2}{d}}\text{dev}(\boldsymbol{b})\end{aligned}$$

where $\boldsymbol{b} = \boldsymbol{F}\boldsymbol{F}^T$ is the left Cauchy-Green strain.

4.2.2 Volumetric stress

$$\begin{aligned}\boldsymbol{P}^{\text{vol}} &= \frac{\partial \Psi^{\text{vol}}(J)}{\partial \boldsymbol{F}} = J\Psi^{\text{vol}\prime}(J)\boldsymbol{F}^{-T} \\ \boldsymbol{\tau}^{\text{vol}} &= J\Psi^{\text{vol}\prime}(J)\boldsymbol{I}\end{aligned} \tag{17}$$

4.2.3 Total stress

Ultimately, we have the total stress and its deviatoric part $\boldsymbol{s}$:

$$\boldsymbol{\tau} = \mu J^{E,-2/d}\text{dev}(\boldsymbol{b}^E) + \Psi^{\text{vol}\prime}(J^E)J^E\boldsymbol{I} \tag{18}$$

$$\boldsymbol{s} = \text{dev}(\boldsymbol{\tau}) = \mu J^{E,-2/d}\text{dev}(\boldsymbol{b}^E) \tag{19}$$

since $\text{dev}(\boldsymbol{I}) = 0$ and $\text{dev}(\text{dev}(\boldsymbol{A})) = \text{dev}(\boldsymbol{A})$ for any matrix $\boldsymbol{A}$.

4.3 Stress derivative

4.3.1 Deviatoric stress derivative

Applying the differential operator to both sides of Eqn. (16), we get:

$$\begin{aligned}\delta\boldsymbol{P}^{\text{dev}} =&\delta\left(\mu J^{2a}(a\boldsymbol{F}:\boldsymbol{F}\boldsymbol{F}^{-T}+\boldsymbol{F})\right)\\ =&2a\mu J^{2a-1}\delta J(a\boldsymbol{F}:\boldsymbol{F}\boldsymbol{F}^{-T}+\boldsymbol{F})\\ &+\mu J^{2a}\left(2a\boldsymbol{F}:\delta\boldsymbol{F}\boldsymbol{F}^{-T}+a\boldsymbol{F}:\boldsymbol{F}\delta(\boldsymbol{F}^{-T})+\delta\boldsymbol{F}\right)\\ =&2a\mu J^{2a}\boldsymbol{F}^{-T}:\delta F(a\boldsymbol{F}:\boldsymbol{F}\boldsymbol{F}^{-T}+\boldsymbol{F})\\ &+\mu J^{2a}\left(2a\boldsymbol{F}:\delta\boldsymbol{F}\boldsymbol{F}^{-T}+a\boldsymbol{F}:\boldsymbol{F}\delta(\boldsymbol{F}^{-T})+\delta\boldsymbol{F}\right).\end{aligned}$$

We can compute $\delta\boldsymbol{F}^{-T}$ by applying differential operator to $(\boldsymbol{F}\boldsymbol{F}^{-1})^T=\boldsymbol{I}$ as:

$$\begin{aligned}\delta\left((\boldsymbol{F}\boldsymbol{F}^{-1})^T\right)&=\delta\boldsymbol{I}=0\\ \delta\boldsymbol{F}^{-T}\boldsymbol{F}^T+\boldsymbol{F}^{-T}\delta\boldsymbol{F}^T&=0\\ \delta\boldsymbol{F}^{-T}=-\boldsymbol{F}^{-T}\delta\boldsymbol{F}^T\boldsymbol{F}^{-T}&=-(\boldsymbol{F}^{-1}\delta\boldsymbol{F}\boldsymbol{F}^{-1})^T.\end{aligned}$$

Thus, we have:

$$\begin{aligned}\delta\boldsymbol{P}^{\text{dev}} =&2a\mu J^{2a}\boldsymbol{F}^{-T}:\delta F(a\boldsymbol{F}:\boldsymbol{F}\boldsymbol{F}^{-T}+\boldsymbol{F})\\ &+\mu J^{2a}\left(2a\boldsymbol{F}:\delta\boldsymbol{F}\boldsymbol{F}^{-T}-a\boldsymbol{F}:\boldsymbol{F}(\boldsymbol{F}^{-1}\delta\boldsymbol{F}\boldsymbol{F}^{-1})^T+\delta\boldsymbol{F}\right).\end{aligned}$$

4.3.2 Volumetric stress derivative

Similarly, applying the differential operator to both sides of Eqn. (17), we get:

$$\begin{aligned}\delta\boldsymbol{P}^{\text{vol}}&=\delta\left(J\Psi^{\text{vol}\prime}(J)\boldsymbol{F}^{-T}\right)\\ &=\delta J\Psi^{\text{vol}\prime}(J)\boldsymbol{F}^{-T}+J\delta(\Psi^{\text{vol}\prime}(J))\boldsymbol{F}^{-T}+J\Psi^{\text{vol}\prime}(J)\delta(\boldsymbol{F}^{-T})\\ &=\delta J\Psi^{\text{vol}\prime}(J)\boldsymbol{F}^{-T}+J\delta J\Psi^{\text{vol}\prime\prime}(J)\boldsymbol{F}^{-T}+J\Psi^{\text{vol}\prime}(J)\delta(\boldsymbol{F}^{-T}).\end{aligned}$$

5 Plasticity

To discuss the plasticity theory, we need first to decompose the deformation gradient into two parts

$$\boldsymbol{F}=\boldsymbol{F}^E\boldsymbol{F}^P.$$

Only the elastic part, $\boldsymbol{F}^E$, contributes to the elastic potential energy and the corresponding elastic forces.

Consider principal stress space: for a pure elastic material, principal stress can reside at any point, indicating either compression or tension. However, for plastic materials, only a subset of the whole stress space is admissible: this is called the yield surface. When a material's stress remains inside of the yield surface, it behaves exactly as an elastic object. However, when stress happens to cross the surface due to discretized time integration, we must find a direction to project it back onto the surface. Using our non-associated method the direction is relatively easy to find, but the exact distance of projection is trickier. In the following subsections, for each material, we will discuss the corresponding yield surface, projection direction, and projection distance, respectively.

5.1 The basics

We define the left elastic Cauchy-Green strain and right plastic Cauchy-Green strain,

$$\begin{aligned}\boldsymbol{b}^E&=\boldsymbol{F}^E\boldsymbol{F}^{E^T}\\ \mathbf{C}^P&=\boldsymbol{F}^{P^T}\boldsymbol{F}^P\end{aligned}$$

and they relate to each other via

$$\boldsymbol{b}^E = \boldsymbol{F}\mathbf{C}^{P^{-1}}\boldsymbol{F}^T.$$

Consider the evolution of $\boldsymbol{b}^E$:

$$\begin{aligned}\frac{D\boldsymbol{b}^E}{Dt} &= \frac{D(\boldsymbol{F}\mathbf{C}^{P^{-1}}\boldsymbol{F}^T)}{Dt} \\ &= \frac{D\boldsymbol{F}}{Dt}\mathbf{C}^{P^{-1}}\boldsymbol{F}^T + \boldsymbol{F}\mathbf{C}^{P^{-1}}\frac{D\boldsymbol{F}^T}{Dt} + \boldsymbol{F}\frac{D\mathbf{C}^{P^{-1}}}{Dt}\boldsymbol{F}^T. \end{aligned} \tag{20}$$

We apply an operator splitting scheme similar to the one used in incompressible fluid simulation [4] to compute the updated $\boldsymbol{b}^E$.

In Step 1, the first two terms in Eqn. (20) can be used to compute an intermediate solution $\hat{\boldsymbol{b}}^E$ by solving

$$\frac{D\boldsymbol{b}^E}{Dt} = \frac{D\boldsymbol{F}}{Dt}\mathbf{C}^{P^{-1}}\boldsymbol{F}^T + \boldsymbol{F}\mathbf{C}^{P^{-1}}\frac{D\boldsymbol{F}^T}{Dt}. \tag{21}$$

In practice, we simply perform a "trial" elastic step to get $\hat{\boldsymbol{b}}^E = \boldsymbol{b}^{E,\mathrm{tr}}$.

In Step 2, we need to solve

$$\frac{D\boldsymbol{b}^E}{Dt} = \boldsymbol{F}\frac{D\mathbf{C}^{P^{-1}}}{Dt}\boldsymbol{F}^T \tag{22}$$

with the intermediate solution as the initial value condition. To simplify the problem, we can define the Lie derivative of $\boldsymbol{b}^E$ to be the remaining part, and give it a specific form

$$\mathcal{L}_{\boldsymbol{v}}\boldsymbol{b}^E := \boldsymbol{F}\frac{D\mathbf{C}^{P^{-1}}}{Dt}\boldsymbol{F}^T = -2\gamma\boldsymbol{G}\boldsymbol{b}^E. \tag{23}$$

In this way, different flow directions can be achieved simply by applying different $\boldsymbol{G}$. The most general two choices are $\boldsymbol{G} = \frac{\partial y}{\partial \boldsymbol{\tau}}$ for associated flow, and $\boldsymbol{G} = \mathrm{dev}(\frac{\partial y}{\partial \boldsymbol{\tau}})$ for non-associated flow where $y(\boldsymbol{\tau})$ defines the yield surface. Given a particular direction, we can then compute the flow distance needed to move the material back to the yield surface.

There are two ways to solve the ODE:

1. **Exponential integrator:** [11] and [1] take this approach and write

$$\boldsymbol{b}^{E,n+1} = e^{-2\delta\gamma\boldsymbol{G}}\boldsymbol{b}^{E,\mathrm{tr}}. \tag{24}$$

2. **Backward Euler:** In [3] and [15], the ODE is discretized as

$$\boldsymbol{b}^{E,n+1} - \boldsymbol{b}^{E,\mathrm{tr}} = -2\delta\gamma\boldsymbol{G}\boldsymbol{b}^{E,n+1}. \tag{25}$$

Notice the unknown $\delta\gamma$ represents the distance we want to solve. In this paper, we choose the second method to do the projection. We can expand the right side to get

$$\boldsymbol{b}^{E,n+1} - \boldsymbol{b}^{E,\mathrm{tr}} = -2\delta\gamma\boldsymbol{G}[\mathrm{dev}(\boldsymbol{b}^{E,n+1}) + \frac{1}{d}\mathrm{tr}(\boldsymbol{b}^{E,n+1})\boldsymbol{I}] \tag{26}$$

As proved in [11], it becomes much more convenient to resolve plasticity projection in the diagonal space of the deformation gradient. From here on, we assume all variables, such as $\boldsymbol{b}$, $\boldsymbol{G}$, τ, $\boldsymbol{s}$, etc., are in diagonal space.

Here we define the pressure p from the Kirchhoff stress

$$p = -\frac{1}{d}tr(\boldsymbol{\tau}).$$

It represents the value projected to the hydrostatic axis in stress space. We further define q as the value corresponding to the axis orthogonal to the hydrostatic axis by

$$q = \sqrt{\frac{6-d}{2}}\|\boldsymbol{s}\|$$

A pair of p and q can be used to replace the original Kirchhoff stress to represent the yield surface as $y(p, q) = 0$.

We list some key equations here:

$$\frac{\partial p}{\partial \boldsymbol{\tau}} = -\frac{1}{d}\mathbf{1}$$

$$\begin{aligned}\frac{\partial q}{\partial \boldsymbol{\tau}} &= \frac{\partial q}{\partial \boldsymbol{s}} : \frac{\partial \boldsymbol{s}}{\partial \boldsymbol{\tau}} \\ &= \sqrt{\frac{6-d}{2}}\frac{\boldsymbol{s}}{\|\boldsymbol{s}\|}\end{aligned}$$

5.2 Cam Clay

We adopt the definition of the Cohesive Cam Clay (CCC) yield surface from [7]

$$y(p, q) = q^2(1 + 2\beta) + M^2(p + \beta p_0)(p - p_0)$$

where β is the cohesion coefficient, M controls the friction; meanwhile, p_0 relates to the hardening required to deliver the correct behavior of particular materials and has the form

$$p_0 = Ksinh(\xi \max(-\alpha, 0)) \tag{27}$$

where $K = \frac{2}{3}\mu + \lambda$ is the bulk modulus, ξ is the hardening factor, and α is a hardening parameter we use to track our fracture-friendly hardening (it is initialized to be $log(J^P)$ but will not always be equal, see §5.2.2).

We rewrite the Kirchhoff stress here, but now with the superscript E:

$$\boldsymbol{\tau} = \mu J^{E,-\frac{2}{d}}\mathrm{dev}(\boldsymbol{b}^E) + J^E\Psi^{\mathrm{vol}\prime}(J^E)\mathbf{1}.$$

So,

$$\begin{aligned}\frac{\partial y}{\partial \boldsymbol{\tau}} &= 2q(1 + 2\beta)\frac{\partial q}{\partial \boldsymbol{\tau}} + M^2(p - p_0)\frac{\partial p}{\partial \boldsymbol{\tau}} + M^2(p + \beta p_0)\frac{\partial p}{\partial \boldsymbol{\tau}} \\ &= 2q(1 + 2\beta)\sqrt{\frac{6-d}{2}}\frac{\boldsymbol{s}}{\|\boldsymbol{s}\|} - \frac{M^2(2p + (\beta - 1)p_0)}{d}\mathbf{1}.\end{aligned}$$

Now we compute $\boldsymbol{G}$.

$$\begin{aligned}\boldsymbol{G} &= \mathrm{dev}(\frac{\partial y}{\partial \boldsymbol{\tau}}) \\ &= 2q(1 + 2\beta)\sqrt{\frac{6-d}{2}}\frac{\boldsymbol{s}}{\|\boldsymbol{s}\|}\end{aligned}$$

Rewrite Eqn. (26) by replacing $\mathrm{dev}(\boldsymbol{b}^{E,n+1}) = \frac{1}{\mu}(J^E)^{\frac{2}{d}}\boldsymbol{s}$ from Eqn. (19),

$$\boldsymbol{b}^{E,n+1} - \boldsymbol{b}^{E,\mathrm{tr}} = -2\delta\gamma\boldsymbol{G}[\mathrm{dev}(\boldsymbol{b}^{E,n+1}) + \frac{1}{d}\mathrm{tr}(\boldsymbol{b}^{E,n+1})\mathbf{1}] \tag{28}$$

The first term is assumed to be small when we only consider simulating relatively stiff materials; thus, we have

$$\begin{aligned}\boldsymbol{b}^{E,n+1} - \boldsymbol{b}^{E,\mathrm{tr}} &= -q(1+2\beta)\sqrt{6-d}\frac{1}{d}\mathrm{tr}(\boldsymbol{b}^{E,n+1})\delta\gamma\frac{\boldsymbol{s}}{\|\boldsymbol{s}\|} \\ &= -q(1+2\beta)\sqrt{6-d}\frac{1}{d}\mathrm{tr}(\boldsymbol{b}^{E,n+1})\delta\gamma\frac{\mu J^{-\frac{2}{d}}\mathrm{dev}(\boldsymbol{b}^{E,n+1})}{\|\boldsymbol{s}\|}.\end{aligned}$$

By appling dev() operator to both sides, and replacing $\mathrm{dev}(\boldsymbol{b}^{E,n+1}) = \frac{1}{\mu}(J^E)^{\frac{2}{d}}\boldsymbol{s}$, it is easy to see $\boldsymbol{s}^{\mathrm{tr}}()$ and $\boldsymbol{s}^{n+1}$ are vectors in the same direction, i.e.,

$$\frac{\boldsymbol{s}^{n+1}}{\|\boldsymbol{s}^{n+1}\|} = \frac{\boldsymbol{s}^{\mathrm{tr}}}{\|\boldsymbol{s}^{\mathrm{tr}}\|}. \tag{29}$$

By applying tr operator to both sides, we get

$$\mathrm{tr}(\boldsymbol{b}^{E,n+1}) = \mathrm{tr}(\boldsymbol{b}^{E,\mathrm{tr}}). \tag{30}$$

We apply the non-associated flow rule, which implies the plasticity preserves volume $(J^P)^{n+1} = (J^P)^{\mathrm{tr}}$. Furthermore, the total deformation gradient is also not changed by plasticity projection. Thus $(J^E)^{n+1} = (J^E)^{\mathrm{tr}}$, and $p^{n+1} = p^{\mathrm{tr}}$. So we rewrite y as follows noting that we have also substituted in $q^{n+1} = \sqrt{\frac{6-d}{2}}||s^{n+1}||$:

$$y = \frac{6-d}{2}\|\boldsymbol{s}^{n+1}\|^2(1+2\beta) + M^2(p^{\mathrm{tr}} + \beta p_0)(p^{\mathrm{tr}} - p_0) = 0. \tag{31}$$

Note that this expression for y does not always have a solution and is dependent on our value of p^{tr}. More specifically, we compare our computed p^{tr} with the known minimum and maximum p values that lie on the ellipsoid: $p_{\max} = p_0$ and $p_{\min} = -\beta p_0$. These can be derived easily using the fact that on the p-axis we know $q = 0$ meaning that the entire first term is 0.

Fortunately, with this new expression for y, we have everything we need to compute $\boldsymbol{b}^{E,n+1}$ and thus $\boldsymbol{F}^{n+1}$. At this point, we have $\boldsymbol{b}^{E,\mathrm{tr}}$, so we can use this to compute p^{tr} as follows:

$$p^{\mathrm{tr}} = -\frac{1}{d}\mathrm{tr}\left(\mu J^{E,\frac{-2}{d}}\mathrm{dev}(\boldsymbol{b}^{E,\mathrm{tr}}) + J^{E,\mathrm{tr}}\Psi^{vol'}(J^{E,\mathrm{tr}})\mathbf{1}\right) = -J^{E,\mathrm{tr}}\Psi^{vol'}(J^{E,\mathrm{tr}}).$$

Now that we have p^{tr}, we must use this value to determine which of three cases we must use to proceed with any further computation. The cases are broken down as follows and are graphically illustrated in Fig. 2:

- **Case 1:** $p^{\mathrm{tr}} > p_0$
- **Case 2:** $p^{\mathrm{tr}} < -\beta p_0$
- **Case 3:** $-\beta p_0 < p^{\mathrm{tr}} < p_0$

In this section we will assume that we have found that we are within the p range associated with Case 3 (see next subsection for Case 1 and Case 2).

With p^{tr} we may compute $||\boldsymbol{s}^{n+1}||$ using Eqn. (31) as shown below:

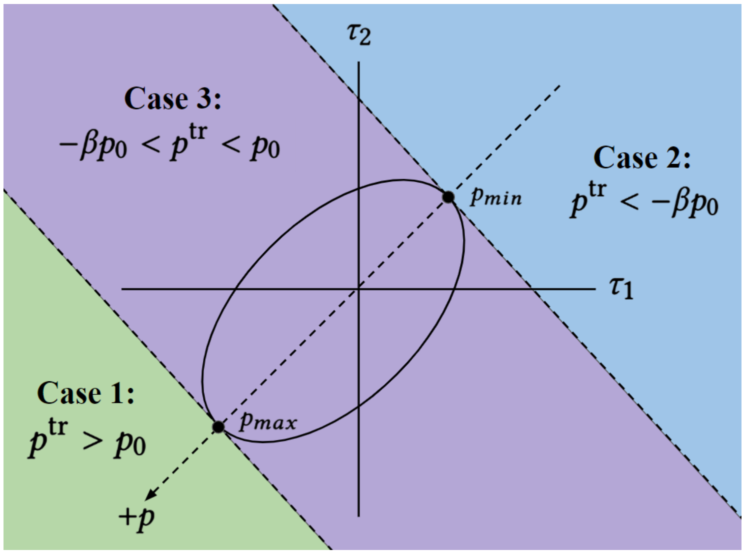

Figure 2: **Projection Cases.** Non-Associated Cam Clay yield surface shown in 2D Kirchhoff stress space with each of the three possible cases highlighted for clarity

$$||\boldsymbol{s}^{n+1}|| = M\sqrt{\frac{2(p^{\text{tr}} + \beta p_0)(p^{\text{tr}} - p_0)}{(d-6)(1+2\beta)}}.$$

Now, using Eqn. (29) we can compute $\boldsymbol{s}^{n+1}$ from $||\boldsymbol{s}^{n+1}||$ as follows:

$$\boldsymbol{s}^{n+1} = \frac{\boldsymbol{s}^{\text{tr}}}{||\boldsymbol{s}^{\text{tr}}||}||\boldsymbol{s}^{n+1}||.$$

Now, using Eqn. (41) we can use $\boldsymbol{s}^{n+1}$ to find $\text{dev}(\boldsymbol{b}^{E,n+1})$:

$$\text{dev}(\boldsymbol{b}^{E,n+1}) = \frac{\boldsymbol{s}^{n+1}}{\mu J^{\frac{-2}{d}}}.$$

Additionally, from Eqn. (30) we see that with our computed $\boldsymbol{b}^{E,\text{tr}}$ we can compute the desired $\text{tr}(\boldsymbol{b}^{E,n+1})$ as follows:

$$\text{tr}(\boldsymbol{b}^{E,n+1}) = \text{tr}(\boldsymbol{b}^{E,\text{tr}}) = \text{tr}(\boldsymbol{F}^{E,\text{tr}}\boldsymbol{F}^{E,\text{tr}^T}).$$

Now that we have both $\text{dev}(\boldsymbol{b}^{E,n+1})$ and $\text{tr}(\boldsymbol{b}^{E,n+1})$ we can reformulate the definition of the deviatoric operator to solve for $\boldsymbol{b}^{E,n+1}$ as below:

$$\boldsymbol{b}^{E,n+1} = \text{dev}(\boldsymbol{b}^{E,n+1}) + \frac{1}{d}\text{tr}(\boldsymbol{b}^{E,n+1})\mathbf{1}.$$

Finally, now that we have $\boldsymbol{b}^{E,n+1}$ we can at last compute the desired $\boldsymbol{F}^{E,n+1}$ based on the definition of $\boldsymbol{b}$:

$$\boldsymbol{F}^{E,n+1} = \boldsymbol{b}^{E,n+1}(\boldsymbol{F}^{E,n+1})^{-T}.$$

5.2.1 Case 1 and Case 2

Recall that Eqn. (31) does not always have a solution. Particularly, when $p^{\text{tr}} > p_0$ or $p^{\text{tr}} < -\beta p_0$, there is no solution. In these two cases we need to project to the tips of the ellipsoid. More specifically for each case:

- **Case 1:** $p^{n+1} = p_{\max} = p_0$
- **Case 2:** $p^{n+1} = p_{\min} = -\beta p_0$

With these values for p^{n+1}, we can compute $J^{E,n+1}$ by plugging Eqn. (18) into the definition of p and then subsequently plugging in $\Psi^{\text{vol}\prime}$ to get the following compact expression (note the trace of the first term is 0 in Eqn. (18)):

$$J^{E,n+1} = \sqrt{\frac{-2p^{n+1}}{\kappa} + 1}. \tag{32}$$

Thus, we can compute $J^{E,n+1}$ for each case like so:

- **Case 1:** $J^{E,n+1} = \sqrt{\frac{-2p_0}{\kappa} + 1}$
- **Case 2:** $J^{E,n+1} = \sqrt{\frac{2\beta p_0}{\kappa} + 1}$

Finally, we can reconstruct the principal stretch as:

$$\Sigma^{E,n+1} = (J^{E,n+1})^{\frac{1}{d}}\boldsymbol{I}.$$

.

5.2.2 Hardening

In order to track hardening, we focus on updating the volumetric and shear plastic deformation with a hardening parameter α. For the first two cases, where dilational motion is dominant, α encodes changes in $log(J^P)$, which again can be achieved by using the relationship between the decomposed deformation gradient before and after the second ODE solve: $F = F^{E,\text{tr}}F^{P,n} = F^{E,n+1}F^{P,n+1}$

We can take the determinant of both sides to get the following relationship that allows us to straightforwardly update α:

$$\alpha^{n+1} = \log(\frac{J^{E,\text{tr}}}{J^{E,n+1}}) + \alpha^n \tag{33}$$

As such, in cases 1 and 2 we can simply update α by adding $log(J^{E,\text{tr}}/J^{E,n+1})$ to it since it already contains the value of the previous α.

However, in case 3, we have plastic flow enduring pure shearing, and our non-associated flow rule does not change J^P, making this simple hardening inapplicable. Instead, we propose a novel approach that allows volume-preserving fractures to occur under pure shearing while still updating the yield surface with appropriate hardening. It is inspired by the observation that on the larger p side of the ellipsoid, we want to enforce material hardening, and on the other side, material softening (allowing natural fracture). Therefore, we define the intersection point $(p^\times, q^\times)$ to be the common point shared both by the yield surface ellipsoid and by the line connecting the trial state $(p^{\text{tr}}, q^{\text{tr}})$ and the ellipsoid center (p^c, q^c) (see Fig. 3). Specifically, the form of the line is as follows:

$$(p^\times, q^\times) = (p^c, q^c) + l\frac{(p^c, q^c) - (p^{\text{tr}}, q^{\text{tr}})}{||(p^c, q^c) - (p^{\text{tr}}, q^{\text{tr}})||}.$$

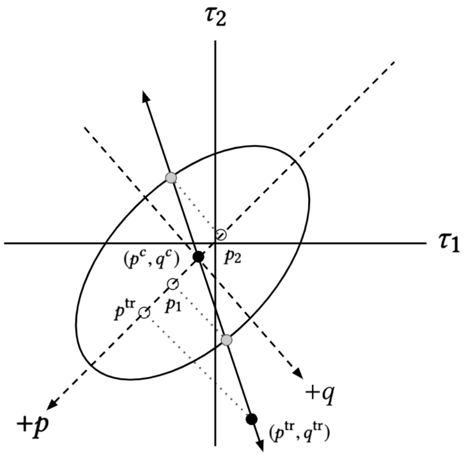

Figure 3: **Case 3 Hardening.** Illustration of our fracture-friendly hardening for Case 3 hardening of the yield surface. The grey points represent intersections between the line from $(p^{\text{tr}}, q^{\text{tr}})$ to (p^c, q^c) and the yield surface itself. We choose between p_1 and p_2 by determining which one is on the same side as p^{tr}.

Additionally, we can formulate the yield surface in terms of these intersection points as shown below:

$$0 = {q^{\times}}^2(1 + 2\beta) + M^2(p^{\times} + \beta p_0)(p^{\times} - p_0).$$

With these two equations we can plug the first into the second to get a quadratic equation of the form:

$$Al^2 + Bl + C = 0.$$

Once we have expressions for A, B, and C, we can simply use the quadratic formula to find our two solutions for l. Further, it is useful to define the two components of the direction vector in terms of p and q separately. We will call these D_p and D_q respectively and they have the following forms:

$$D_p = \frac{p^c - p^{\text{tr}}}{||(p^c, q^c) - (p^{\text{tr}}, q^{\text{tr}})||},$$

$$D_q = \frac{q^c - q^{\text{tr}}}{||(p^c, q^c) - (p^{\text{tr}}, q^{\text{tr}})||}.$$

With these defined, the expressions for A, B, and C are straightforward to compute with one additional detail about q^c. Since the center of the ellipse is on the p-axis, we know that $q^c = 0$ and this will help us reduce the expressions for A,B,C even further. These coefficients take the following form:

$$A = M^2 D_p^2 + D_q^2(1 + 2\beta),$$

$$B = M^2 D_p(2p^c - p_0 + \beta p_0),$$

$$C = M^2(p^c + \beta p_0)(p^c - p_0).$$

Once we have the coefficients, we can use the quadratic formula to compute two solutions l_1 and l_2. Then, we may use these to get our candidate values for $p^{\times}$ through the expression:

$$(p_i, q_i) = (p^c, q^c) + l_i \frac{(p^c, q^c) - (p^{\text{tr}}, q^{\text{tr}})}{||(p^c, q^c) - (p^{\text{tr}}, q^{\text{tr}})||}$$

With this, we get two values p_1 and p_2. In order to determine which of the solutions we want, we use a simple sign test to determine which point is on the same side of the center as p^{tr}. More specifically, we keep the one which fulfills $(p^{\mathrm{tr}} - p^c)(p^\times - p^c) > 0$. Choosing the correct side of the ellipsoid captures the damage caused by shearing, and triggers more intensive softening when the shearing happens quickly.

From $p^\times$ we can compute $J^{E,\times}$, which is employed to perform the update to α similar to the first two cases as $\log(\frac{J^{E,\mathrm{tr}}}{J^{E,\times}})$. Note that the reason we introduce the variable α is that in this hardening case α is no longer the true $\log(J^P)$ but instead a hardening state variable that we track.

5.3 von Mises

In the case of von Mises, we have

$$\begin{aligned}
y(\boldsymbol{\tau}) &= \sqrt{\boldsymbol{s} : \boldsymbol{s}} - \sqrt{\frac{2}{6-d}}\boldsymbol{\tau}_y, \\
\boldsymbol{s} &= \boldsymbol{\tau} - \frac{1}{d}\mathrm{tr}(\boldsymbol{\tau}), \\
\frac{\partial y}{\partial \boldsymbol{s}} &= \frac{\boldsymbol{s}}{\|\boldsymbol{s}\|}, \\
\frac{\partial y}{\partial \boldsymbol{\tau}} &= \frac{\boldsymbol{s}}{\|\boldsymbol{s}\|},
\end{aligned}$$

where the last equality can be shown with chain rule.

We then adopt the BE discretization of the flow rule (Eqn. 25): $\boldsymbol{b}^{E,n+1} - \boldsymbol{b}^{E,\mathrm{tr}} = -2\delta\gamma \boldsymbol{G}(\boldsymbol{b}^{E,n+1})\boldsymbol{b}^{E,n+1}$, where $\boldsymbol{G} = \frac{\partial y}{\partial \boldsymbol{\tau}} = \frac{\boldsymbol{s}}{\|\boldsymbol{s}\|}$. Therefore

$$\boldsymbol{b}^{E,n+1} - \boldsymbol{b}^{E,\mathrm{tr}} = -2\delta\gamma \boldsymbol{G}^{n+1}\left(\mathrm{dev}(\boldsymbol{b}^{E,n+1}) + \frac{1}{d}\mathrm{tr}(\boldsymbol{b}^{E,n+1})\mathbf{1}\right).$$

Further plugging in the result from our energy that $\boldsymbol{s} = \mu J^{E,-2/d}\mathrm{dev}(\boldsymbol{b}^E)$, it becomes

$$\begin{aligned}
\boldsymbol{b}^{E,n+1} - \boldsymbol{b}^{E,\mathrm{tr}} &= -2\delta\gamma\frac{\boldsymbol{s}}{\|\boldsymbol{s}\|}\left(\frac{\boldsymbol{s}}{\mu J^{E,-2/d}} + \frac{1}{d}\mathrm{tr}(\boldsymbol{b}^{E,n+1})\mathbf{1}\right) \\
&= -2\delta\gamma J^{E,2/d}\frac{\boldsymbol{s}}{\|\boldsymbol{s}\|}\frac{\boldsymbol{s}}{\|\boldsymbol{s}\|}\frac{\|\boldsymbol{s}\|}{\mu} - 2\delta\gamma\frac{1}{d}\mathrm{tr}(\boldsymbol{b}^{E,n+1})\frac{\boldsymbol{s}}{\|\boldsymbol{s}\|}.
\end{aligned}$$

According to [16], the first term is close to 10^{-3} for most metals, and thus can be neglected. Thus

$$\boldsymbol{b}^{E,n+1} - \boldsymbol{b}^{E,\mathrm{tr}} = -2\delta\gamma\frac{1}{d}\mathrm{tr}(\boldsymbol{b}^{E,n+1})\frac{\boldsymbol{s}^{n+1}}{\|\boldsymbol{s}^{n+1}\|}. \tag{34}$$

Talking its dev() and tr() give

$$\begin{aligned}
\mathrm{dev}(\boldsymbol{b}^{E,n+1}) - \mathrm{dev}(\boldsymbol{b}^{E,\mathrm{tr}}) &= -2\delta\gamma\frac{1}{d}\mathrm{tr}(\boldsymbol{b}^{E,n+1})\frac{\boldsymbol{s}^{n+1}}{\|\boldsymbol{s}^{n+1}\|} \qquad (35) \\
\mathrm{tr}(\boldsymbol{b}^{E,n+1}) - \mathrm{tr}(\boldsymbol{b}^{E,\mathrm{tr}}) &= 0. \qquad (36)
\end{aligned}$$

Plugging Eqn 19 and Eqn 36 into Eqn 35 gives

$$\frac{1}{\mu J^{E,-2/d}}(\boldsymbol{s}^{n+1} - \boldsymbol{s}^{\mathrm{tr}}) = -2\delta\gamma\frac{1}{d}\mathrm{tr}(\boldsymbol{b}^{E,\mathrm{tr}})\frac{\boldsymbol{s}^{n+1}}{\|\boldsymbol{s}^{n+1}\|}, \tag{37}$$

which reveals $\boldsymbol{s}^{n+1}$ and $\boldsymbol{s}^{\mathrm{tr}}$ are along the same direction, i.e.,

$$\frac{\boldsymbol{s}^{n+1}}{\|\boldsymbol{s}^{n+1}\|} = \frac{\boldsymbol{s}^{\mathrm{tr}}}{\|\boldsymbol{s}^{\mathrm{tr}}\|}.$$

Plugging this back into Eqn. (37) gives

$$\frac{1}{\mu J^{E,-2/d}}(\frac{\boldsymbol{s}^{\text{tr}}}{\|\boldsymbol{s}^{\text{tr}}\|}\|\boldsymbol{s}^{n+1}\| - \boldsymbol{s}^{\text{tr}}) = -2\delta\gamma\frac{1}{d}\text{tr}(\boldsymbol{b}^{E,\text{tr}})\frac{\boldsymbol{s}^{\text{tr}}}{\|\boldsymbol{s}^{\text{tr}}\|}.$$

Combining this with yield function $\|\boldsymbol{s}^{n+1}\| - \sqrt{\frac{2}{6-d}}\boldsymbol{\tau}_y = 0$ allows us to solve for $\delta\gamma$ analytically:

$$\|\boldsymbol{s}^{\text{tr}}\| - \frac{2}{d}J^{E,-2/d}\mu\text{tr}(\boldsymbol{b}^{E,\text{tr}})\delta\gamma = \sqrt{\frac{2}{6-d}}\boldsymbol{\tau}_y. \tag{38}$$

After getting $\delta\gamma$, we can reconstruct $\boldsymbol{b}^{E,n+1}$ (and thus $\boldsymbol{F}^{E,n+1}$) using

$$\boldsymbol{b}^{E,n+1} - \boldsymbol{b}^{E,\text{tr}} = -2\delta\gamma\frac{1}{d}\text{tr}(\boldsymbol{b}^{E,\text{tr}})\frac{\boldsymbol{s}^{\text{tr}}}{\|\boldsymbol{s}^{\text{tr}}\|}. \tag{39}$$

5.4 Drucker Prager

We present here important, related equations:

$$\boldsymbol{\tau} = \mu J^{E,-2/d}\text{dev}(\boldsymbol{b}^E) + \Psi^{\text{vol}'}(J^E)J^E\mathbf{1} \tag{40}$$

$$\boldsymbol{s} = \text{dev}(\boldsymbol{\tau}) = \mu J^{E,-2/d}\text{dev}(\boldsymbol{b}^E) \tag{41}$$

$$y = c_f\text{tr}(\boldsymbol{\tau}) + \|\text{dev}(\boldsymbol{\tau})\| - c_c \tag{42}$$

$$\frac{\partial y}{\partial \boldsymbol{\tau}} = c_f\mathbf{1} + \frac{\boldsymbol{s}}{\|\boldsymbol{s}\|} \tag{43}$$

$$\boldsymbol{G} = \text{dev}(\frac{\partial y}{\partial \boldsymbol{\tau}}) = \frac{\boldsymbol{s}}{\|\boldsymbol{s}\|} \tag{44}$$

Following the same steps as in von Mises, we get the same flow rule (Eqn. 34) by making an assumption of a small $\boldsymbol{s}/\mu$ term,

$$\begin{aligned}
\boldsymbol{b}^{E,n+1} - \boldsymbol{b}^{E,\text{tr}} &= -2\delta\gamma\frac{1}{d}\text{tr}(\boldsymbol{b}^{E,n+1})\frac{\boldsymbol{s}^{n+1}}{\|\boldsymbol{s}^{n+1}\|} \\
\text{dev}(\boldsymbol{b}^{E,n+1}) - \text{dev}(\boldsymbol{b}^{E,\text{tr}}) &= -2\delta\gamma\frac{1}{d}\text{tr}(\boldsymbol{b}^{E,n+1})\frac{\boldsymbol{s}^{n+1}}{\|\boldsymbol{s}^{n+1}\|} \\
\text{tr}(\boldsymbol{b}^{E,n+1}) - \text{tr}(\boldsymbol{b}^{E,\text{tr}}) &= 0 \\
\frac{1}{\mu J^{E,-2/d}}(\boldsymbol{s}^{n+1} - \boldsymbol{s}^{\text{tr}}) &= -2\delta\gamma\frac{1}{d}\text{tr}(\boldsymbol{b}^{E,\text{tr}})\frac{\boldsymbol{s}^{n+1}}{\|\boldsymbol{s}^{n+1}\|} \\
\frac{\boldsymbol{s}^{n+1}}{\|\boldsymbol{s}^{n+1}\|} &= \frac{\boldsymbol{s}^{\text{tr}}}{\|\boldsymbol{s}^{\text{tr}}\|} \\
\frac{1}{\mu J^{E,-2/d}}(\frac{\boldsymbol{s}^{\text{tr}}}{\|\boldsymbol{s}^{\text{tr}}\|}\|\boldsymbol{s}^{n+1}\| - \boldsymbol{s}^{\text{tr}}) &= -2\delta\gamma\frac{1}{d}\text{tr}(\boldsymbol{b}^{E,\text{tr}})\frac{\boldsymbol{s}^{\text{tr}}}{\|\boldsymbol{s}^{\text{tr}}\|}.
\end{aligned}$$

From $\boldsymbol{\tau} = \mu J^{E,-2/d}\text{dev}(\boldsymbol{b}^E) + \Psi^{\text{vol}'}(J^E)J^E\mathbf{1}$ we know

$$\text{tr}(\boldsymbol{\tau}^{n+1}) = \text{tr}(\boldsymbol{\tau}^{\text{tr}})$$

by noticing that $J^{E,n+1} = J^{E,\text{tr}}$ due to our volume-preserving plasticity construction. Further using this property in the yield function $0 = c_f\text{tr}(\boldsymbol{\tau}^{n+1}) + \|\boldsymbol{s}^{n+1}\| - c_c$ we know

$$\|\boldsymbol{s}^{n+1}\| = c_c - c_f\text{tr}(\boldsymbol{\tau}^{\text{tr}}).$$

This allows us to write the equation for $\delta\gamma$:

$$\|\boldsymbol{s}^{\mathrm{tr}}\| - \frac{2}{d}J^{E,-2/d}\mu\mathrm{tr}(\boldsymbol{b}^{E,\mathrm{tr}})\delta\gamma = c_c - c_f\mathrm{tr}(\boldsymbol{\tau}^{\mathrm{tr}}) \tag{45}$$

$$\boldsymbol{b}^{E,n+1} - \boldsymbol{b}^{E,\mathrm{tr}} = -\delta\gamma\frac{2}{d}\mathrm{tr}(\boldsymbol{b}^{E,\mathrm{tr}})\frac{\boldsymbol{s}^{\mathrm{tr}}}{\|\boldsymbol{s}^{\mathrm{tr}}\|}. \tag{46}$$

5.5 Condition for Volume Preserving Plasticity

Here, we derive the condition that $J^P = 1$ (plastic flow is volume-preserving).

Theorem 1 $J^P = 1$ *is equivalent to* $tr(\boldsymbol{F}^E\dot{\boldsymbol{F}^P}\boldsymbol{F}^{P^{-1}}\boldsymbol{F}^{E^{-1}}) = 0$

$$\dot{J^P} = J^P\boldsymbol{F}^{P^{-T}} : \dot{\boldsymbol{F}^P},$$
$$\mathrm{tr}(\boldsymbol{F}^E\dot{\boldsymbol{F}^P}\boldsymbol{F}^{P^{-1}}\boldsymbol{F}^{E^{-1}}) = \boldsymbol{F}^{P^{-T}} : \dot{\boldsymbol{F}^P}.$$

Theorem 2 *For isotropic elasticity,* $\boldsymbol{\tau}\boldsymbol{b}^E = \boldsymbol{b}^E\boldsymbol{\tau}$ *and* $\boldsymbol{\tau}\boldsymbol{b}^{E^{-1}} = \boldsymbol{b}^{E^{-1}}\boldsymbol{\tau}$

This can be easily seen by writing $\boldsymbol{\tau} = 2\Psi_I\boldsymbol{b}^E + 4\Psi_{II}\boldsymbol{b}^{E^2} + 2III_{\boldsymbol{b}^E}\Psi_{III}\boldsymbol{I}$ and noticing that both $\boldsymbol{\tau}$ and $\boldsymbol{b}^E$ are symmetric [2].

Now, we follow Chapter 7 of [2] to introduce notations. We can define $\dot{w}$ to be the internal rate of work per unit initial volume done by the stress. I.e.,

$$\dot{w} = \boldsymbol{\tau} : \boldsymbol{l},$$

where $\boldsymbol{l}$ is the velocity gradient $\boldsymbol{l} = \dot{\boldsymbol{F}}\boldsymbol{F}^{-1}$. According to Example 7.1 of [2] (which uses Theorem 2), it can be proven that

$$\dot{w} = \boldsymbol{\tau} : \boldsymbol{l} = \frac{1}{2}\boldsymbol{\tau} : \left(\left.\frac{d\boldsymbol{b}^E}{dt}\right|_{\mathbf{C}^P=const}\boldsymbol{b}^{E^{-1}}\right).$$

Example 7.2 of [2] further proves that

$$\boldsymbol{l}^E := \dot{\boldsymbol{F}^E}\boldsymbol{F}^{E^{-1}}$$
$$\dot{w^E} = \boldsymbol{\tau} : \boldsymbol{l}^E = \boldsymbol{\tau} : \left(\frac{1}{2}\frac{d\boldsymbol{b}^E}{dt}\boldsymbol{b}^{E^{-1}}\right).$$

Then $\boldsymbol{l}^P$ can be introduced by showing (see Eqn 7.17 of [2])

$$\dot{w^P} = \boldsymbol{\tau} : \boldsymbol{l}^P$$
$$\boldsymbol{l}^P := -\frac{1}{2}\left.\frac{d\boldsymbol{b}^E}{dt}\right|_{\boldsymbol{F}=const}\boldsymbol{b}^{E^{-1}}$$
$$= -\frac{1}{2}\mathcal{L}_{\boldsymbol{v}}(\boldsymbol{b}^E)\boldsymbol{b}^{E^{-1}}.$$

According to Example 7.3 of [2],

$$\boldsymbol{l}^P := -\frac{1}{2}\left.\frac{d\boldsymbol{b}^E}{dt}\right|_{\boldsymbol{F}=const}\boldsymbol{b}^{E^{-1}}$$
$$= \frac{1}{2}\boldsymbol{F}\mathbf{C}^{P^{-1}}\dot{\mathbf{C}^P}\boldsymbol{F}^{-1}.$$

And it is easy to prove using index notation that

$$\mathrm{tr}(\frac{1}{2}\boldsymbol{F}\mathbf{C}^{P^{-1}}\dot{\mathbf{C}^P}\boldsymbol{F}^{-1}) = \mathrm{tr}(\boldsymbol{F}^E\dot{\boldsymbol{F}^P}\boldsymbol{F}^{P^{-1}}\boldsymbol{F}^{E^{-1}}).$$

Therefore, according to Theorem 1 we know $\mathrm{tr}(\boldsymbol{l}^P) = 0$ implies $J^P = 1$. Note that in our plasticity, $\boldsymbol{l}^P = \gamma\boldsymbol{G}$. Thus, choosing a trace-free $\boldsymbol{G}$ guarantees $J^P = 1$.

6 Local vs. Non-local CDM

In the main paper we refer to the advantages and challenges local and non-local continuum damage methods pose [18], and we present more concrete comparisons here for further discussion. Local continuum damage mechanics models have shown to be effective for meshed fracture simulation, but the crack propagation produced is notoriously dependent on mesh resolution and direction [8]. However, it is unclear whether this effect is present when paired with a meshless discretization method such as MPM. As such, here we compare the stress threshold based local damage approach outlined in [6] with our phase field method to show the advantages of our non-local damage phase field formulation (specifically within the realm of MPM discretization).

6.1 Fracture Modes

To capture mode 1 (Fig. 4) and mode 2 (Fig. 5) fractures with local and non-local damage approaches, we follow experimental setups popular in mechanics. In each demo the material is a 0.4 by 0.4 square with $E = 1000$, $\nu = 0.25$, and $\rho = 2$. In all demos, the local CDM strain limit is $\sigma_F = 5$, the non-local CDM energy release rate is $\mathcal{G} = 3.00 \times 10^{-3}$, the mobility constant set to $M_c = 0$ for ease of comparison, and the regularization parameter set to $l_0 = 0.4\Delta x$. In Fig. 4 and Fig. 5 $\Delta x = 0.005$ and $\Delta t = 8 \times 10^{-5}$. The key difference between mode 1 and mode 2 setups lies in the boundary configuration. For mode 1 fracture, the material is given an additional 0.02 units of material in the y direction above and below the square; this material is added so that a sticky boundary can be inserted in the material and hold onto these added material “handles.” The top boundary moves up with speed 0.05, and the bottom boundary moves at the same speed, but downwards. Conversely, for mode 2 fracture, there is only one moving boundary; the top boundary touches the top of the original square but uses MPM sticky collision to cause friction as this boundary moves to the right at speed 0.025. There are two additional directional boundaries added for mode 2: a bottom boundary that touches the bottom of the original square with MPM slippery collision, and a half-height boundary on the bottom left to hold the bottom left portion of the square in place. This configuration effectively gives the intraplanar opposing forces we associate with mode 2 fracture.

First, we present the comparison between local and non-local damage for mode 1 in Fig. 4. Though this mode of fracture does appear to be captured by both methods, the local damage approach produces jagged and less visually-plausible paths than the smooth, continuous crack tip formed through our PFF approach. Similarly, in Fig. 5 we observe again that both methods qualitatively appear to capture mode 2 fracture; however, the crack path simulated with local damage does not follow the typical curvature associated with mode 2 fracture in mechanics, while CD-MPM clearly produces a much smoother and clear curve that more closely matches mode 2 fracture results in mechanics. Note that due to MPM’s treatment of boundaries, the boundaries themselves appear to affect the crack path when it reaches them (note the slight change in curvature at the boundary in both methods). Ultimately, it appears that local damage struggles mainly with capturing mode 2 fracture, while our non-local PFF method qualitatively captures both modes with a smooth crack representation.

6.2 Resolution Dependence

The experiments in Fig. 6 and Fig. 7 use the aforementioned mode 2 fracture configuration with the only changes being Δx and Δt as noted in the figure caption. In these figures we compare local and non-local damage methods for mode 2 fracture at different resolutions. In Fig. 6 there is a clear difference in crack speed propagation: higher resolutions result in faster cracks, demonstrating a strong resolution dependency. Conversely, in Fig. 7, the visually identical crack speed of our non-local damage method shows the resolution invariance of our phase-field approach. Ultimately, it is clear that CD-MPM is free of the resolution dependence we can associate with local damage and this is very likely caused by the regularization parameter, l_0, used in our phase-field formulation to scale the crack radius. Through this observation, we chose to always set l_0 based on some proportion of simulation Δx ($l_0 = 0.5\Delta x$ was often sufficient). Thus, we have shown that under the MPM discretization scheme, local CDM is in fact grid resolution dependent while the phase-field non-local approach is MPM grid resolution invariant.

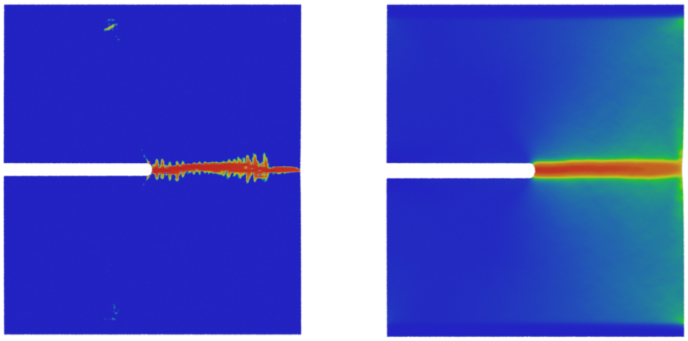

Figure 4: **Mode 1 Fracture.** (Left) Local CDM produces jagged, unnatural mode 1 fracture; (Right) Our non-local CDM approach produces a smooth, continuous crack tip for mode 1 fracture

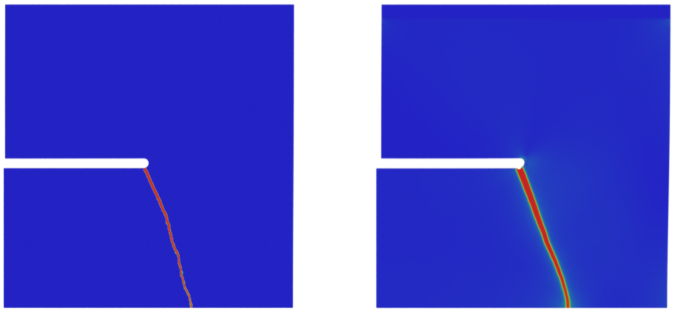

Figure 5: **Mode 2 Fracture.** (Left) Local CDM produces a jagged crack path that has little curvature we expect from mode 2 fracture; (Right) Our non-local CDM approach produces a smooth crack front with clear curvature that echoes classical mode 2 fracture results.

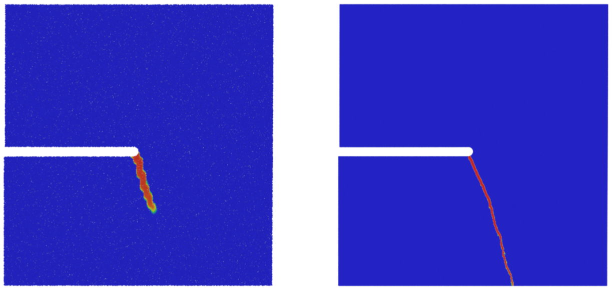

Figure 6: **Local CDM Resolution Dependency.** (Left) Local CDM run for mode 2 fracture at $\Delta x = 0.01$ and $\Delta t = 4 \times 10^{-5}$. Note the crack has not propagated to the boundary yet; (Right) Local CDM run for mode 2 fracture at $\Delta x = 0.0025$ and $\Delta t = 1.6 \times 10^{-6}$. Note that here, the crack has reached the boundary indicating that higher resolutions (lower Δx) lead to faster crack propagation for local CDM methods.

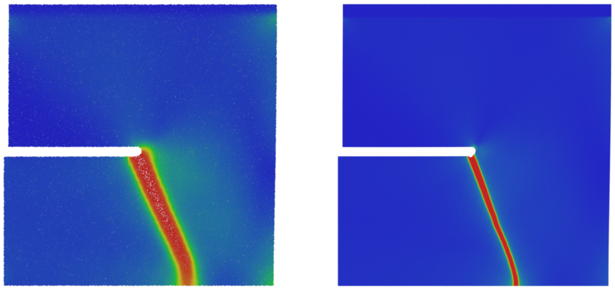

Figure 7: **Non-Local CDM Resolution Invariance.** (Left) Non-local CDM run for mode 2 fracture at $\Delta x = 0.01$ and $\Delta t = 4 \times 10^{-5}$. Note the crack tip (saturated red region) has propagated to the boundary; (Right) Non-local CDM run for mode 2 fracture at $\Delta x = 0.0025$ and $\Delta t = 1.6 \times 10^{-6}$. Note that the crack tip has also just reached the boundary here, indicating that our non-local CDM method is resolution invariant.

References

[1] F. Auricchio and R.L. Taylor. A return-map algorithm for general associative isotropic elasto-plastic materials in large deformation regimes. *International Journal of Plasticity*, 15(12):1359–1378, 1999.

[2] J. Bonet and R. Wood. *Nonlinear continuum mechanics for finite element analysis.* Cambridge University Press, 2008.

[3] M. J. Borden, T. J.R. Hughes, C. M. Landis, A. Anvari, and I. J. Lee. A phase-field formulation for fracture in ductile materials: Finite deformation balance law derivation, plastic degradation, and stress triaxiality effects. *Computer Methods in Applied Mechanics and Engineering*, 312:130–166, 2016.

[4] R. Bridson. *Fluid simulation for computer graphics.* Taylor & Francis, 2008.

[5] K. Cahill. *Physical mathematics.* Cambridge University Press, 2013.

[6] M. Cervera and M. Chiumenti. Mesh objective tensile cracking via a local continuum damage model and a crack tracking technique. *Computer Methods in Applied Mechanics and Engineering*, 196(1-3):304–320, 2006.

[7] J. Gaume, T. Gast, J. Teran, A. van Herwijnen, and C. Jiang. Dynamic anticrack propagation in snow. *Nature communications*, 9(1):3047, 2018.

[8] P. Grassl and M. Jirásek. On mesh bias of local damage models for concrete. 01 2004.

[9] Y. Hu, Y. Fang, Z. Ge, Z. Qu, Y. Zhu, A. Pradhana, and C. Jiang. A moving least squares material point method with displacement discontinuity and two-way rigid body coupling. *ACM Transactions on Graphics (TOG)*, 37(4):150, 2018.

[10] C. Jiang, C. Schroeder, J. Teran, A. Stomakhin, and A. Selle. The material point method for simulating continuum materials. In *ACM SIGGRAPH 2016 Course*, pages 24:1–24:52, 2016.

[11] G. Klár, T. Gast, A. Pradhana, C. Fu, C. Schroeder, C. Jiang, and J. Teran. Drucker-prager elasto-plasticity for sand animation. *ACM Trans Graph*, 35(4):103:1–103:12, 2016.

[12] C. Kuhn and R. Müller. A continuum phase field model for fracture. *Engineering Fracture Mechanics*, 77(18):3625–3634, 2010.

[13] L. D. Landau and E. M. Lifshitz. The classical theory of fields. 1971.

[14] R. Radovitzky and M. Ortiz. Error estimation and adaptive meshing in strongly nonlinear dynamic problems. *Computer Methods in Applied Mechanics and Engineering*, 172(1-4):203–240, 1999.

[15] J. C. Simo. A framework for finite strain elastoplasticity based on maximum plastic dissipation and the multiplicative decomposition: Part i. continuum formulation. *Computer methods in applied mechanics and engineering*, 66(2):199–219, 1988.

[16] J.C. Simo and C. Miehe. Associative coupled thermoplasticity at finite strains: Formulation, numerical analysis and implementation. *Computer Methods in Applied Mechanics and Engineering*, 98(1):41–104, 1992.

[17] A. Stomakhin, C. Schroeder, C. Jiang, L. Chai, J. Teran, and A. Selle. Augmented MPM for phase-change and varied materials. *ACM Trans Graph*, 33(4):138:1–138:11, 2014.

[18] J. Wolper, Y. Fang, M. Li, J. Lu, M. Gao, and C. Jiang. CD-MPM: Continuum damage material point methods for dynamic fracture animation. *ACM Trans. Graph.*, 38(4), July 2019.

[19] Y. Yue, B. Smith, P. Y. Chen, M. Chantharayukhonthorn, K. Kamrin, and E. Grinspun. Hybrid grains: Adaptive coupling of discrete and continuum simulations of granular media. In *SIGGRAPH Asia 2018 Technical Papers*, SIGGRAPH Asia '18, pages 283:1–283:19, 2018.